



IoT-based hydrological monitoring of water-induced landslides: a case study in central Norway

Emir Ahmet Oguz¹ · Ivan Depina^{2,5} · Bård Myhre³ · Graziella Devoli⁴ · Helge Rustad³ · Vikas Thakur¹

Received: 31 December 2021 / Accepted: 21 April 2022
© The Author(s) 2022

Abstract

Water-induced landslides pose a great risk to the society in Norway due to their high frequency and capacity to evolve in destructive debris flows. Hydrological monitoring is a widely employed method to understand the initiation mechanism of water-induced landslides under various climate conditions. Hydrological monitoring systems can provide relevant information that can be utilized in landslide early warning systems to mitigate the risk by issuing early warnings. These monitoring systems can be significantly enhanced, and wider deployments can be achieved through the recent developments within the domain of the Internet of Things (IoT). Therefore, this study aims to demonstrate a case study on an automated hydrological monitoring system supported by the IoT-based state-of-the-art technologies employing public mobile networks. Volumetric water content (VWC) sensors, suction sensors, and piezometers were used in the hydrological monitoring system to monitor the hydrological activities. The monitoring system was deployed in a case study area in central Norway at two locations of high susceptible geological units. During monitored period, the IoT-based hydrological monitoring system provided novel and valuable insights into the hydrological response of slopes to seasonally cold climates in terms of VWC and matric suction. The effects of rainfall, snow melting, ground freezing, and thawing were captured. The current study also made an attempt to integrate the collected data into a physical-based landslide susceptibility model to obtain a more consistent and reliable hazard assessment.

Keywords Hydrological monitoring · IoT · Water-induced · Landslide · Rainfall · Snow melt

Introduction

A landslide is defined as the downslope movement of soil, rock, and organic materials under the effects of gravity. The adverse consequences of landslides such as fatalities, injuries to people, economic losses, and environmental damages

are well known and documented in the literature (Froude and Petley 2018; Haque et al. 2019; Lacasse et al. 2010; Nadim et al. 2006; Petley 2012). According to the statistics of the Centre for Research on the Epidemiology of Disasters (CRED 2021), the Emergency Events Database, retrieved in November 2021, roughly 488,000 deaths happened since 2000 due to natural hazards associated with landslides, which also includes ground movement due to earthquakes. According to the database, the overall value of damages and economic losses, directly or indirectly related to landslides, was estimated to be over US\$ 310 billion since 2000.

Landslides can be triggered by a wide range of factors including rainfall, snow melt, earthquakes, human activities, erosion, or a combination of different phenomena. Among different triggering factors, water is mainly involved in the majority of slope destabilizations (Michoud et al. 2013; Pecoraro et al. 2018). Water-induced landslides are one of the major hazards in Norway due to their high frequency on hillsides and capacity to turn into a high-speed destructive debris flow. They might be triggered by extreme rainfall

✉ Emir Ahmet Oguz
emir.a.oguz@ntnu.no

¹ Department of Civil and Environmental Engineering, Norwegian University of Science and Technology, NO-7491 Trondheim, Norway

² Department of Rock and Geotechnical Engineering, SINTEF, Torgarden, 4760, NO-7465 Trondheim, Norway

³ Department of Connectivity Technologies and Platforms, SINTEF, Torgarden, 4760, NO-7465 Trondheim, Norway

⁴ Norwegian Water Resources and Energy Directorate (NVE), Middelthuns Gate 29, 0368 Oslo, Norway

⁵ Faculty of Civil Engineering, Architecture, and Geodesy, University of Split, Matice hrvatske 15, 21000 Split, Croatia

events, snow melt, or a combination of rainfall and snow melt. Such water-induced landslides can be initiated due to the increase in the soil water content and increasing soil weight, loss of soil suction, erosion, or artesian pressure.

The slopes in hillsides are usually unsaturated before landslide initiation (Bordoni et al. 2015). The behavior of unsaturated slopes depends highly on volumetric water content (VWC) and corresponding changes in suction (SafeLand 2012). Triggering events such as rainfall or snow melting lead to an increase in VWC and reduction in suction values, both of which are the parameters affecting unsaturated shear strength and eventually stability of the slopes. At the instant of water-induced landslide initiation, initiated slope might be either saturated with positive pore pressure due to perched water table or unsaturated with the presence of suction. Several studies performed hydrological monitoring in hillsides in order to clarify the underlying initiation mechanism of water-induced landslides (Bordoni et al. 2021, 2015; Crawford et al. 2019; Godt et al. 2009; Kim et al. 2021; Smith et al. 2014; Wei et al. 2020). Hydrological monitoring can provide important insights into the hydrological processes occurring in similar slopes (Comegna et al. 2016) such as water infiltration and corresponding changes in VWC and suction (Li et al. 2005).

In the study of Godt et al. (2009), landslide occurrence was reported in a natural slope under partially saturated conditions based on the hydrological monitoring data. The study revealed that VWC and matric suction data can be used to predict the occurrence of partially saturated shallow landslides by employing the method of infinite slope stability for unsaturated conditions (Lu and Godt 2008). Similarly in the literature, the hydrological monitored data on the VWC and suction were excessively employed in combination with the infinite slope stability method for unsaturated conditions to assess the stability condition of slopes (Bordoni et al. 2015; Kim et al. 2021; Wei et al. 2020; Yang et al. 2019). Additionally, Song et al. (2021) employed hydrological monitoring in an early warning system with the hazard levels based on the monitored parameters and corresponding stability assessment.

In this study, we examined a landslide-prone study area in central Norway where the landslide events initiate mainly due to intense rainfall events, snow melting, or a combination of them. To understand the initiation mechanism, hydrological monitoring systems were deployed at two locations with two geological units, which are susceptible to sliding. Hydrological activities were monitored with VWC sensors, suction sensors, and piezometers. In practice, such monitoring systems have been challenging due to conventional monitoring systems including costly sensors, inflexible cable-based systems, limited scalability and flexibility, and regular maintenance. However, new, small, and less expensive types of wireless sensors for monitoring geotechnical

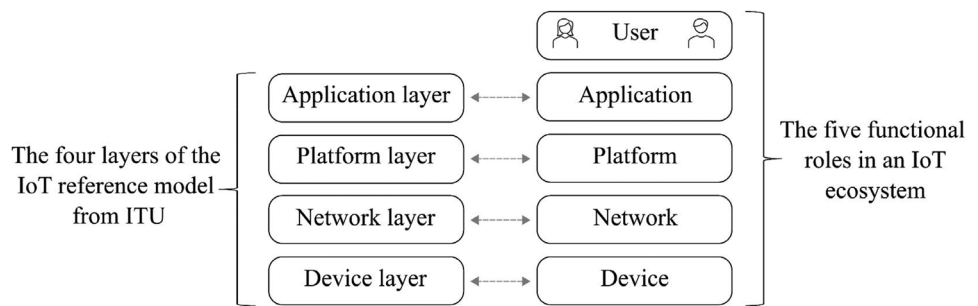
parameters started to emerge in the market, being inspired by the enabling technology of the Internet of Things (IoT). Several research studies on adopting the IoT concept in landslide monitoring (Abraham et al. 2020; Bhosale et al. 2017; Chaturvedi et al. 2018; Hou 2018) indicate that IoT can improve conventional monitoring with the provision of cost efficiency, flexibility, and ease to scale the system. Therefore, the hydrological monitoring system, in this study, was developed based on the state-of-the-art IoT technology employing public mobile networks. This provided more efficient deployment and operation of the monitoring system compared to the conventional systems. The architecture of the developed system was demonstrated by means of functional roles in typical IoT-based systems. Through deployed IoT-based hydrological monitoring system, valuable insights into the hydrological response of the slopes to seasonally cold climate conditions in Norway were obtained. The usage of collected data in landslide prediction over the study area was illustrated through an automated physical-based model, as an attempt to provide a basis for an early warning system.

On this background, the remainder of the paper is structured as follows: the “**Background in IoT**” section provides the background in IoT and the typical system architecture with the functional roles in an IoT ecosystem. This section will serve as a baseline for the IoT application of the current study. In the “**Deployed IoT-based hydrological monitoring system**” section, the deployed IoT-based hydrological monitoring system will be presented. Then, the “**Case study of the IoT-based hydrological monitoring system**” section will present the study area, the deployment of the system in the field, and data acquisition and interpretation of collected data. The “**Data processing and early warning strategies**” section will provide data processing and early warning strategies as an attempt to assess the stability condition over the study area based on collected data via a physical-based model. Finally, the “**Discussion**” section focuses on several discussion points, and the “**Summary**” section summarizes the paper.

Background in IoT

Over the last two decades, employing wireless sensors to monitor hydrological conditions has gradually moved from being an idea towards reality. As an example, Anumalla et al. (2005) pointed out the need for cost-efficient groundwater measurements, suggesting “the development of an infrastructure for acquiring, transferring and analyzing real-time data” using a modified Wi-Fi network. Some 15 years later, several companies now offer wireless groundwater sensor networks, using various wireless solutions (e.g., Trimble Water 2021; Worldsensing 2021). However, the geotechnical community is still lacking a unified and de facto standard

Fig. 1 The four layers of the IoT reference model as defined by ITU (to the left) and the corresponding functional roles in an IoT ecosystem (to the right) (modified after ITU 2012)



for wireless communication, not being anywhere close to the availability in personal communication and Internet access brought forth by Wi-Fi, 3G, and 4G.

For the employment of the IoT within the geotechnical engineering domain, one could benefit from some guidance on the IoT concept. One such guide can be found with the International Telecommunication Union (ITU), which issued a recommendation (ITU 2012) that aimed to provide an overview of the IoT with the main objective of highlighting this important area for future standardization. This recommendation can provide a baseline and reference for IoT applications within the geotechnical engineering domain. ITU (2012) states that the IoT can be perceived as a far-reaching idea with technological and societal implications. This is followed up by a high-level technical overview and generic requirements but without any specific details on technologies or quantifiable characteristics. ITU does however introduce an IoT reference model, consisting of four distinct layers with associated capabilities. Furthermore, ITU extends the IoT reference model with an IoT ecosystem model, adding the human user as an integral part of the IoT ecosystem.

The IoT reference model consists of four distinct layers, shown on the left part of Fig. 1, being the Device, Network, Platform, and Application layers. The Device layer consists of electronic devices that interact with physical objects and the environment, typically being sensors or actuators. These electronic devices will typically use a Network layer to communicate with a Platform layer.¹ The Network layer includes any physical or logical network providing access to a larger communication network (e.g., the Internet). The Platform layer will, on the other side, include any services related to data storage, basic data processing, and device management. This way, the Network layer addresses transportation of data, while the Platform layer addresses storage and processing of data. Finally, the Application layer performs application-specific processing, evaluation, and presentation, based on data retrieved from the Platform layer.

In the IoT ecosystem model, shown on the right side of Fig. 1, the four layers from the IoT reference model are transformed into four roles that cover the exact same functionality as the layers. These roles are conveniently called Device, Network, Platform, and Application. However, the ecosystem model also introduces a fifth role, the User,² who receives information from the Application role. Although the addition of the User role may seem both trivial and obvious, this extension explicitly acknowledges that no system can be regarded complete without a beneficiary. It also directs attention to the importance of addressing user needs when developing any technical system. Therefore, this study will use the IoT ecosystem model as a reference on how to understand and develop any IoT system.

Deployed IoT-based hydrological monitoring system

Figure 2 illustrates an overall concept of IoT-based hydrological monitoring and early warning system with the five functional roles in an IoT ecosystem shown in Fig. 1. In the Device layer, the sensors should be selected based on the triggering mechanism of the landslides and are responsible for sensing, actuating, controlling, and monitoring activities (Ray 2018). The monitored data is transferred to the Platform layer by the Network layer, which may involve different technologies depending on the network solutions, e.g., public mobile networks, satellite services, or unlicensed wireless technologies such as LoRa, Sigfox, and Wireless M-Bus. The Platform layer can then serve as a provider of data for hydrological monitoring and early warning systems, based on either local or cloud-based data storage and basic processing services. In the Application layer, the data from the Platform layer might be used to assess the stability conditions of a single slope or, more generally, slopes over a landslide-prone region. This can be done by relating the collected data to the stability conditions by defining threshold

¹ Note that ITU references the “Platform layer” as “Service support and Application support layer”.

² Note that ITU references the “User” role as “Application customer”.

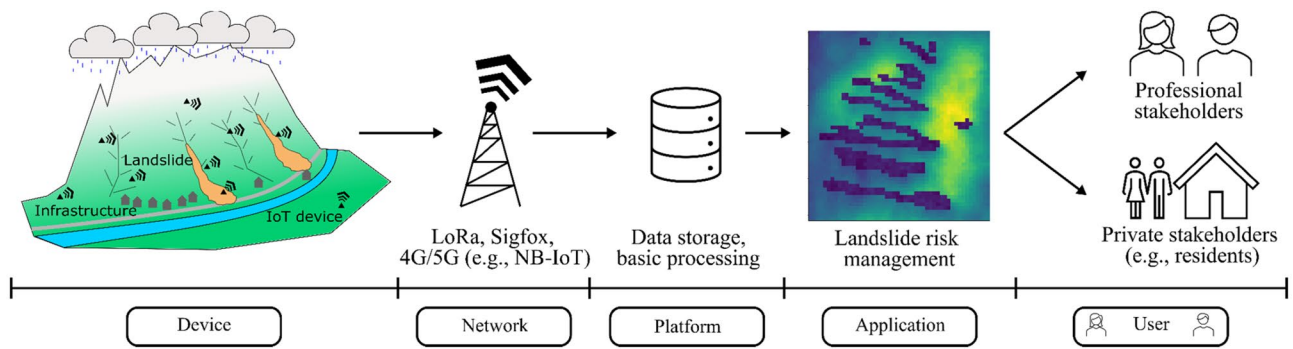


Fig. 2 The overall concept of the IoT-based hydrological monitoring of water-induced landslides and early warning systems (modified after Oguz et al. 2019)

values for different warning levels based on the monitored parameters or by utilizing physical-based models or data-driven approaches (e.g., machine learning algorithms). The Application issues warnings or transmits the landslide stability conditions to the User. The User could, for instance, be either a professional user representing authorities or infrastructure owners or residents/public that are exposed to the landslide risk in an area of relevance.

This paper focuses mainly on two of the aspects, namely how the Device role can be implemented using public mobile networks and how the collected data can be utilized in the Platform layer to understand the hydrological processes important for the stability of slopes over the study area. The other three roles, Network, Application, and User will play a less prominent part within this paper. However, they are still included to a certain detail as they are essential when it comes to establishing a fully operational IoT ecosystem.

Development of the device, network, and platform

Figure 3 illustrates the developed system architecture through the functional roles for the IoT ecosystem. Representing the Device role in Fig. 3, the IoT Devices were constructed, each consisting of two excitation units supporting one piezometer each, one Sparkfun Thing Plus Artemis microcontroller board providing interfaces to all the external sensors, one Nordic Thingy:91 Prototyping Platform communication module providing 4G connectivity through public mobile networks, and one battery pack providing power to the IoT Device. For each IoT Device, a sensor suite of up to three VWC sensors, three suction sensors, and two piezometers was supported. Each sensor was to be sampled every 15 min, with wireless transmission of the acquired measurements once every hour using the public mobile (4G) network. Furthermore, the IoT devices were required to operate on battery for 12 months without any maintenance. Regarding the selection of communication

solution, the motivation for employing the public mobile network was to investigate how emerging 4G-based IoT technologies, intended for machine-type communication would work in practice, with regard to both technical integration and deployment in the field. Within the 4G/LTE³ standard, Narrowband IoT (NB-IoT) and Long Term Evolution Machine Type Communication (LTE-M) were considered to be the most relevant technologies for long-term sensors, as both are directed at machine-type communication (Höglund et al. 2017). The difference between them lies mainly in flexibility and cost: NB-IoT is focused on low-cost and low-power applications for stationary devices (e.g., sensors), while LTE-M supports higher data rates and handover to neighboring cells at the cost of somewhat higher power consumption (Höglund et al. 2017). This may indicate that NB-IoT is a reasonable choice for geotechnical applications, supporting long-time operation in fixed positions. However, several manufacturers provide combined chipsets for NB-IoT and LTE-M (e.g., Nordic Semiconductor 2021), and within the field of professional geotechnical monitoring, it may be expected that flexibility is more important than extreme low-cost communication. Thus, the Nordic Thingy:91 Prototyping Platform, being built upon the RF9160 System-in-Package by Nordic Semiconductor supporting both LTE-M and NB-IoT, was selected as the communication module for the IoT Device.

Representing the Network role in Fig. 3, the public Mobile network provided wireless 4G coverage in the entire study area. As this service was commercially available at the time of the case study, the project's work on network coverage was limited to acquiring relevant subscriptions with relevant Norwegian national mobile operators and verifying connectivity in the study area. Due to practical issues related

³ The terms 4G and LTE can for all practical purposes be used interchangeably. However, from a technical point of view, "4G" refers to a set of requirements for mobile access, while "LTE" refers to a specific technology that fulfills the "4G" requirements (Dahlman et al. 2016).

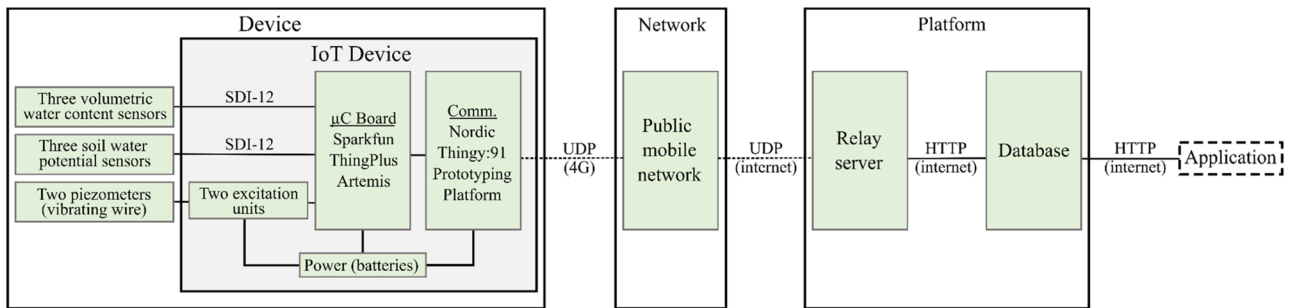


Fig. 3 System architecture and functional roles for the IoT ecosystem, including internal components of the IoT Device (Protocols: UDP: User Datagram Protocol, SDI-12: Serial Data Interface at 1200 baud, and HTTP: Hypertext Transfer Protocol)

to the selected subscriptions and national rollout plans for NB-IoT and LTE-M, the IoT Devices were configured to make use of the LTE-M part of the 4G network.

Representing the Platform role in Fig. 3, the sensor measurements were transmitted to a cloud-based Relay server, implemented on a virtual Linux server. The Relay server received UDP messages from the IoT Devices and forwarded these to a cloud-based database running on a commercial web hotel. The database served as persistent storage for sensor measurements and provided an external application programming interface (API) for downloading sensor measurements over the Internet in CSV format.

For the Application role in Fig. 3, any software that uses the data that has been made available through the database should be regarded as an application. In this paper, the Application role is being manifested by the data processing and early warning strategies with an attempt to assess the stability condition over the study area based on collected data via a physical-based model in the “Data processing and early warning strategies” section.

During the past decade, there have been several developments on IoT-based systems for landslide prediction and early warning with different architectures and varying technologies in Device and Network layers. Some of these studies, e.g., Chaturvedi et al. (2018), Khaing and Thein (2020), Pathania et al. (2020), Soegoto et al. (2021), and Sruthy et al. (2020), showed the feasibility of such IoT-based systems in data acquisition and transfer using different communication technologies. The Application roles in these studies mainly appear as landslide warning systems based on threshold levels inferred from the monitored parameters. In the current study, the physical-based modeling was employed in the Application layer and provided in the “Data processing and early warning strategies” section. In data communication, these studies employed advancements brought forth by wireless solutions, such as Wi-Fi, Bluetooth, and 2G-3G/GSM-based cellular communication. Recent developments in the domain of IoT applications provided new opportunities through a new networking concept, called Low Power

Wide Area Networks (LPWANs). LPWANs address the limitations of abovementioned wireless solutions by providing cost- and power-efficient wireless data transmission over long distances. Several technologies enabling LPWAN deployments have been developed in the last few years (Mekki et al. 2019). Among them, SigFox, LoRa, LTE-M, and NB-IoT can be considered, currently, as leading technologies. In this study, the state-of-art networking solutions, NB-IoT and LTE-M, employing 4G public mobile network were utilized in the Network layer.

Sensors

The selection of sensors for the monitoring system is based on capturing the development of the main triggering conditions for the landslides in the studied area, IoT system constraints, and the implemented landslide modeling strategies. Given that the landslides are mainly triggered by the changes in hydrological conditions in response to rainfall and snow melt events, the selection of sensors is based on monitoring the development of hydrological conditions. The system consists of VWC sensors, suction sensors, and piezometers. Monitoring of surface-water and channel flow was not implemented due to the corresponding sensory solutions requiring power and data transfer exceeding the constraints of the IoT system. Although monitoring snow amounts would be of great value for the project, this was not implemented in the project due to substantial power requirements for such sensory solutions. However, the effects of snow melting and soil thawing on the development of the hydrological conditions are monitored indirectly with the VWC and suction sensors. These sensors provide temperature measurements in addition to the respective measurements of VWC and matric suction. Details on the selected sensors are provided in the following paragraphs.

VWC is measured by soil moisture sensors, TEROS 12 (METER Group 2021a). The sensor sends an electromagnetic field, a 70-MHz oscillating wave to the sensor needles that charge according to the dielectric and VWC of the

surrounding soil medium. The sensor outputs a raw output voltage based on the charging time, which is proportional to the surrounding VWC. Then, the raw output voltage (mV) is converted to the VWC using a calibration equation. Although the manufacturer provides an average calibration equation for mineral soils, the custom calibration equation should be developed for the specific surrounding soil to get more accurate values, as shown in the “Laboratory tests” section.

Matric suction is measured by a soil water potential sensor, i.e., suction sensor, TEROS 21 (METER Group 2021b). The suction sensor measures the water potential in the engineered ceramic discs through the dielectric permittivity. Using the known soil water characteristics (SWCC) of the discs (i.e., the relationship between the VWC and matric suction), the matric suction is calculated. As the suction sensors are not affected by the surrounding soil type but work using the known characteristics of the ceramic discs, calibration for a specific soil type is not necessary. The suction sensor output is directly in kPa, and no conversion is needed. The measurement range is from 9 kPa to the air-dry state. However, the sensor is calibrated to provide the most accurate results in the range of 10 to 100 kPa with the accuracy being $\pm 10\%$. The predictions for drier cases rely on the linear relationship between the water potential and water content on a logarithmic scale.

Piezometers from the M-600 series (Geonor 2021) are used to measure the pore water pressure or groundwater level measurements. The piezometer is a vibrating wire sensor that measures changes in pressure based on changes in the natural frequency of a wire that is connected to a membrane that deforms with varying values of pressure on the membrane. Each piezometer is tested and calibrated in the lab by the manufacturer prior to being shipped for installation. Each of the piezometers is supplied with a calibration chart and a conversion equation to translate the frequency output of the sensor to pore pressure values.

Case study of the IoT-based hydrological monitoring system

Study area

The study area is between Hegra and Meråker located in the county of Trøndelag, central Norway (Fig. 4a). The area is a part of the catchment of the Sjørdal river and is about 200 km² in size. This area was chosen for the implementation of a landslide monitoring system due to being prone to shallow landslide events, with relatively steep slopes, above 20–25°, and having clear evidence of recent landslide events. Additionally, the other reasons for choosing the study area are the availability of nearby weather stations and groundwater measurements and mobile network (4G) coverage.

The bedrock in the study area is composed of Proterozoic and Cambrian metamorphic rocks deformed during the Caledonian orogenesis, covered by a thin cover of Quaternary deposits of different origins (Fig. 4b). A shallow cover of altered bedrock prevails on top of the bedrock in the western sector, formed on-site by physical or chemical decomposition of the bedrock. In the central and eastern sector, the bedrock is covered by an incoherent or thin cover of till deposits (also herein called moraine deposits), picked up, transported, and deposited by glaciers. It is usually hard-packed, poorly sorted, and can contain everything from clay to stone and block. The thickness of these deposits is mainly less than 0.5 m, but it can be much thicker locally. A humus/thin peat cover can be also observed on top of the bedrock with a thickness of 0.2–0.5 m, locally thicker. Rock exposures are frequently visible in this sector. Thick moraine deposits (with a thickness of 0.5 m to several tens of meters) and colluvial deposits left by previous landslides are not particularly representative in the study area and can be observed only locally at a few places. The bottom of the Sjørdal valley is filled with fluvial deposits, with a thickness that varies from 0.5 to more than 10 m, composed of sorted and rounded sand and gravel material. Glaciofluvial deposits are also locally represented and consist of sorted, often sloping layers of different grain sizes. Along the Sjørdal river locally, it is possible to observe marine and fjord deposits, that consist of fine-grained, marine deposits with a thickness from 0.5 m to several tens of meters.

The study area is highly susceptible to different types of landslides in soils, such as debris slides, clay/silty slides, debris avalanches, and debris flows. The area is part of the landslide domain called “Trøndelagkysten” (Devoli and Dahl 2014), where slides in clayey-silty soils are the most frequent landslide types during periods of intense rainfall or rainfall combined with intense snow melting episodes that produce high groundwater and high soil saturation. Debris slides, debris avalanches, and debris flows in moraine deposits were also observed. The high susceptibility of the study area was also confirmed by other landslide susceptibility assessments performed at the national level (Devoli et al. 2019; Fischer et al. 2012). The analysis of the Norwegian national database of mass movements (NVE n.d.), showed that 93 mass movements were registered in the study area between 1750 and 2020. Figure 5 shows the registered landslide events mainly along the main transportation lines with the regional landslide susceptibility levels. Among these registered landslide events, 36 events (35 landslides in soil and 1 slushflow) were triggered by rainfall and snowmelt.

As the majority of soil-related landslide events initiated in fluvial and moraine deposits, both types of Quaternary deposits were selected to be monitored. Following the detailed investigation in the study area, two monitoring

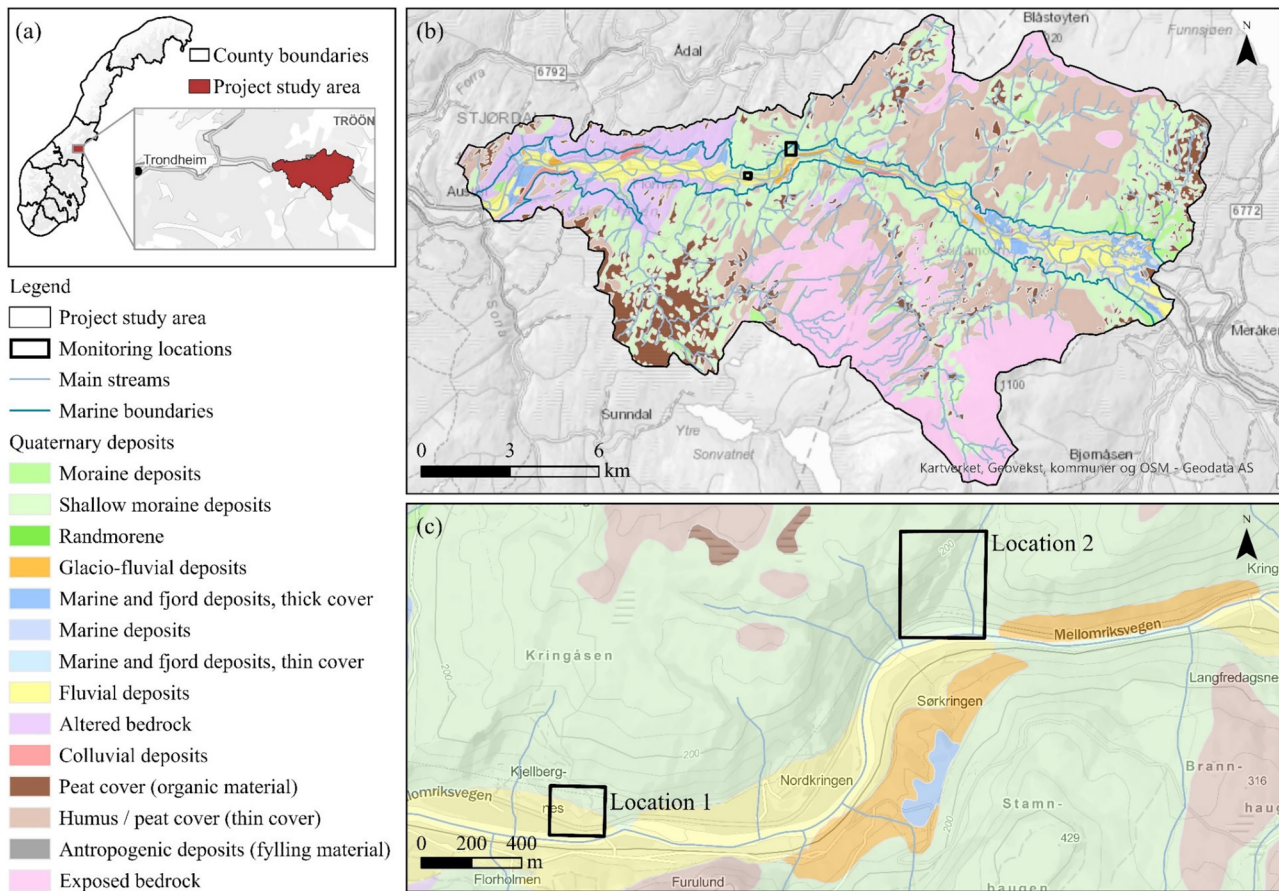


Fig. 4 a Study area in national and regional scale, b Quaternary geology over the study area, and c two selected monitoring locations, Location 1 and Location 2, at detailed scale

locations, which will be called “Location 1” and “Location 2” (Fig. 4c), were selected for further investigation and the installation of IoT-based hydrological monitoring systems.

Location 1, Kjelberget, is a south-facing open slope, ridge form, slightly channelized. The bedrock is covered by the thick fluvial deposit on the hillside towards the bottom of the valley, while a thin cover of moraine deposit appears on the higher parts of the hill (above 80–85 m average sea level). Location 2, Kvernbekkneset, is also a south-facing slope with a clear channelized shape and two main channels that run along this area. The bedrock is covered by moraine deposits that are locally less than 0.5 m thick.

In the national database of mass movements, three landslide events at Location 1 and one landslide event at Location 2 were recorded. Despite being poorly described, the events can be classified as flows and in the category of debris slide in Location 1 and debris flow in Location 2. The events were shallow with a small volume estimated in the range of 5–50 thousand m³. Pictures of the deposits found in newspapers revealed that all events were characterized by high water content. The analysis of hydrometeorological

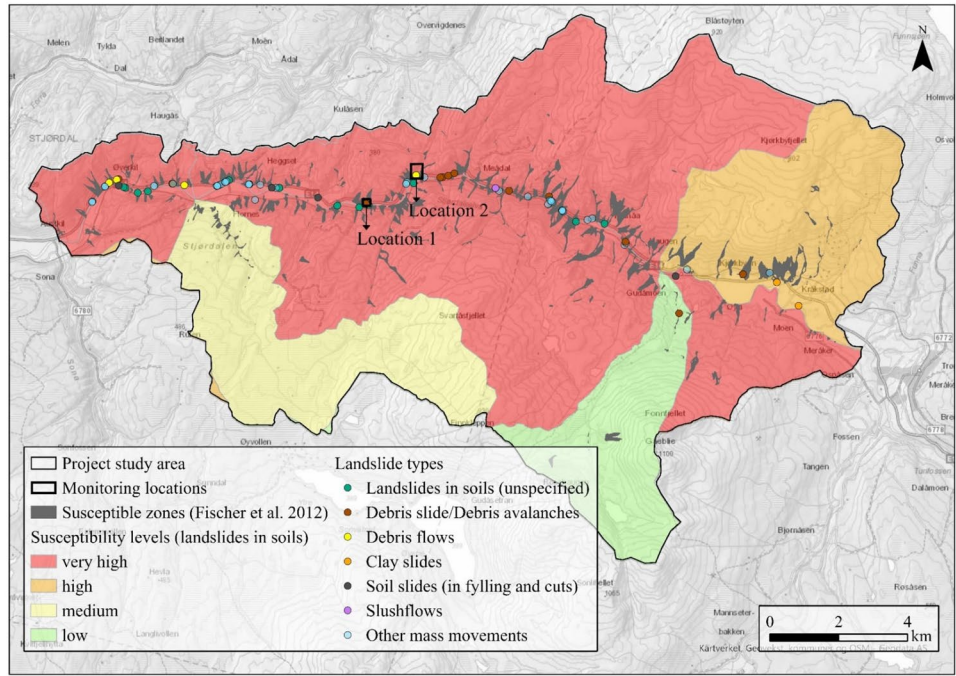
conditions indicated that the landslides in both locations were triggered by intense rainfall, with values between 60 and 80 mm/24 h or by a combination of intense rainfall combined with intense snow melting (40–60 mm/24 h of water supply).

Laboratory tests

For the characterization of the geological units present at the two monitoring locations, i.e., fluvial and moraine deposits, excavation trial pits on intact slopes were constructed, and soil samples were collected for laboratory testing. In situ density measurements were performed for top soil crust with the water replacement test (ASTM D5030/D5030M-21 2021) at Location 1. Additionally, laboratory tests including methods for water content and organic content determination, sieve analysis and hydrometer tests for soil classification, pycnometer test for soil specific gravity, and large-scale direct shear tests were performed.

The measurements of wet in situ density resulted in approximately 13–15 kN/m³ at the top 0.5 m crust at both

Fig. 5 Registered landslide events over the study area with regional susceptibility



locations. At Location 1, the water replacement test resulted in a wet in situ density of 18 kN/m^3 at 0.9 m depth with a gravimetric water content of 8.88%. Additionally, it was observed that the top 20–40 cm crust has much higher organic content than deeper depths at both locations.

Complete grain size distribution curves were obtained for both fluvial and moraine deposits by performing wet sieve analysis and hydrometer tests. Figure 6 shows the grain size distribution curves of both soil types. The fractions of fines, sands, and gravels are 12.9 – 46.3 – 40.8%, respectively, for fluvial deposit and 16.2 – 57.7 – 26.1% for moraine, respectively. The uniformity coefficient (c_u) and coefficient of curvature (c_c) of fluvial deposits are 40.1 and 0.4, respectively,

and of moraine are 29.7 and 0.7, respectively. Both soil types were classified as silty sand according to the European Soil Classification System (ISO 14688–2:2017 2017).

For the VWC sensors, custom calibration equations were developed by recording sensory outputs on samples of fluvial and moraine deposits in a controlled lab environment with known values of VWC. The collected soil samples were saturated at different degrees of saturation level and compacted to satisfy the in situ density measurements. Figure 7 shows the calibration curves for the VWC sensors with the laboratory data and the calibration curve provided by the manufacturer. The results revealed that the raw output voltage values correspond to lower VWC values in comparison

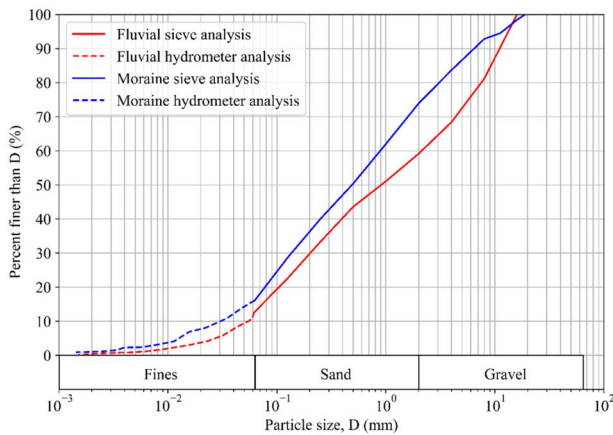


Fig. 6 Grain size distribution of moraine and fluvial deposits

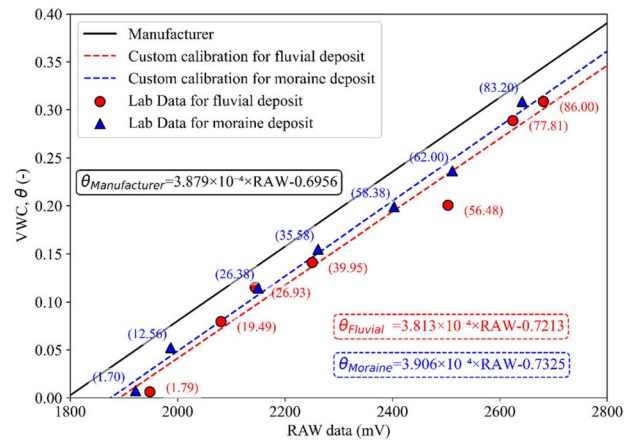


Fig. 7 Calibration chart for VWC sensor

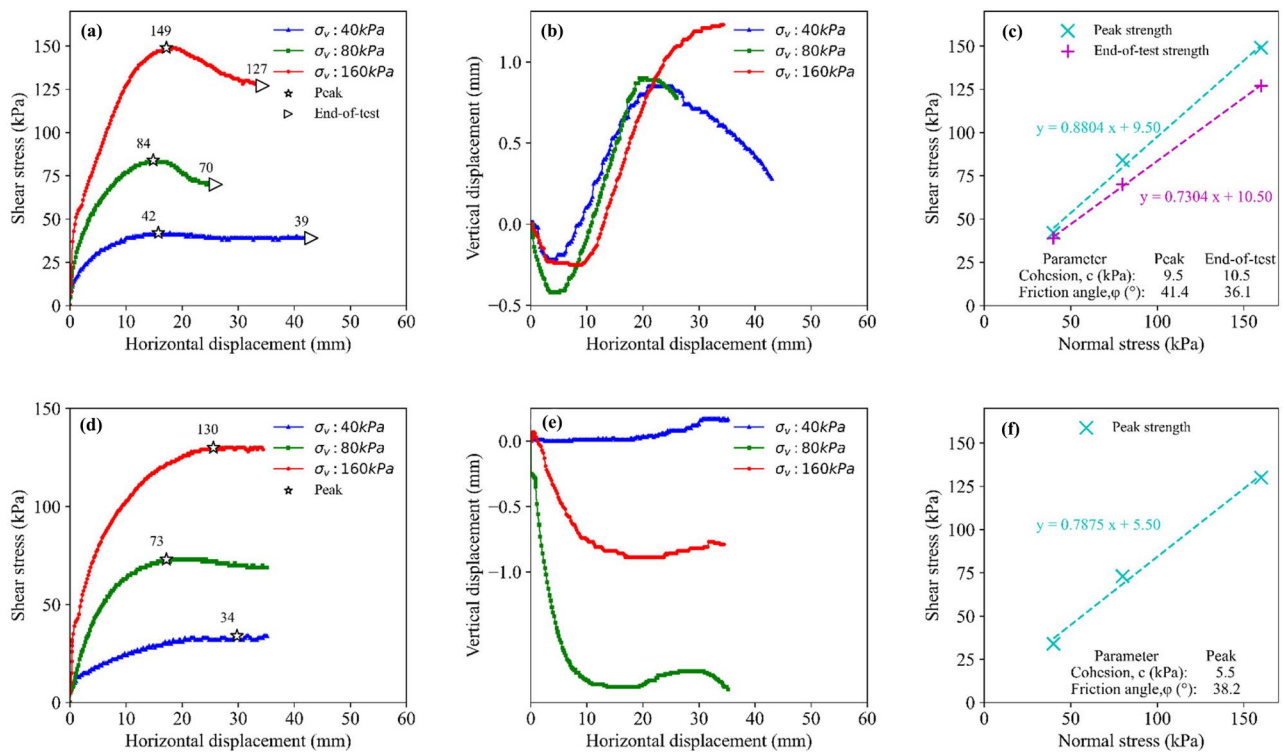


Fig. 8 Large scale direct shear test results for fluvial deposits (a, b, c) and moraine (d, e, f); shear stress data (a, d), vertical displacement data (b, e), and determination of shear strength parameters (c, f)

to the VWC values from the manufacturer’s calibration equation. In Fig. 7, the values in the parentheses are the corresponding degree of saturation, S_r (%), for the soil samples used in the calibration. These custom calibration equations, developed for fluvial and moraine deposits individually, are utilized to convert the sensory reading in mV to the VWC values in m^3m^{-3} .

Large-scale (30 × 30 cm) direct shear tests (ASTM D3080/D3080M–11 2021) were performed to estimate soil strength parameters due to the high fraction of coarse particles. Soil samples were collected from the trial pits at both locations. Soil specimens for each soil type were reconstituted by compacting the samples in the shear box to their in situ density. The tests were conducted at drained conditions with a constant shear strain rate of 1 mm/min. Figure 8 shows the large-scale direct shear test result for fluvial deposits in Fig. 8a–c, and for moraine deposits in Fig. 8d–f. Figure 8a, d shows the shear stress recorded during shearing under different levels of vertical stresses. As the fluvial deposits were in a dense state, a peak and a residual strength have been observed. The vertical displacement data in Fig. 8b also complies with the behavior of a dense soil sample showing an initial contraction and then dilation until the failure. The end-of-test condition was defined as 10–15% strain along the shear plane where shear stress becomes constant and asymptotic to horizontal after the peak. Peak

and end-of-test strength parameters can be seen in Fig. 8c for fluvial deposits, and only peak strength parameters are shown in Fig. 8f for moraine. The results of the large-scale direct shear tests, namely shear strength parameters, were considered in the calibration of the physical-based landslide prediction model, which can be a basis for a landslide early warning system (the “Data processing and early warning strategies” section).

Deployment of the devices in the field

The IoT-based hydrological monitoring systems were deployed at both locations with two monitoring points at each site. Due to the presence of the water channel down the hillside at both locations, the monitoring points were located on both sides of the channels at different elevations to catch possible variations in the hydrological responses along the side of the channel. The monitoring points are shown in Fig. 9b for Location 1 and in Fig. 11b for Location 2. In addition to the two monitoring points, a weather station (Fig. 9d) was installed at Location 1 to monitor the weather conditions.

The VWC and suction sensor were placed within the top 1 m of the soil as the deposits in Location 2 were observed to be locally thin, with the thickness being below 1 m. These sensors were implemented at three depths at both locations

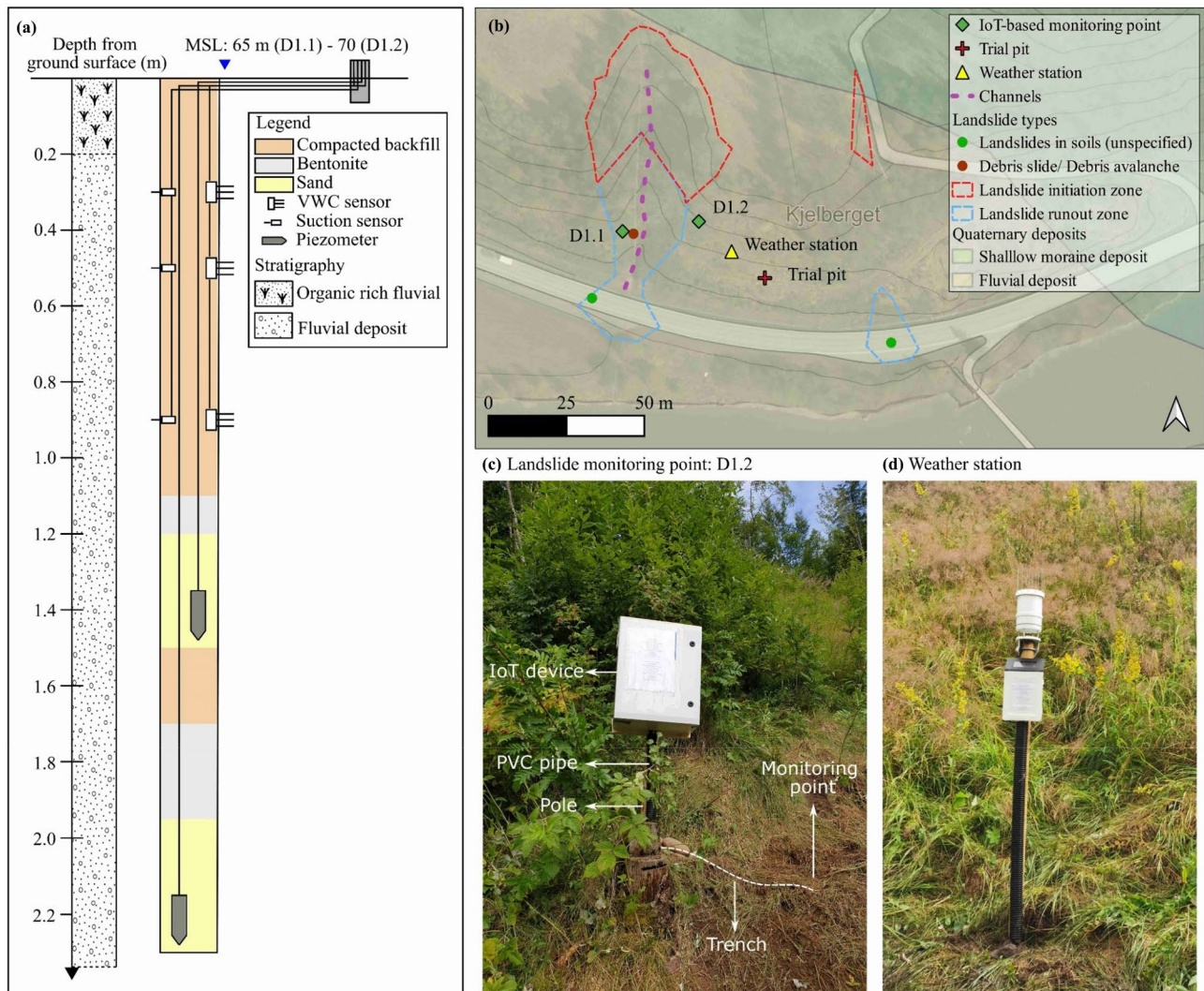


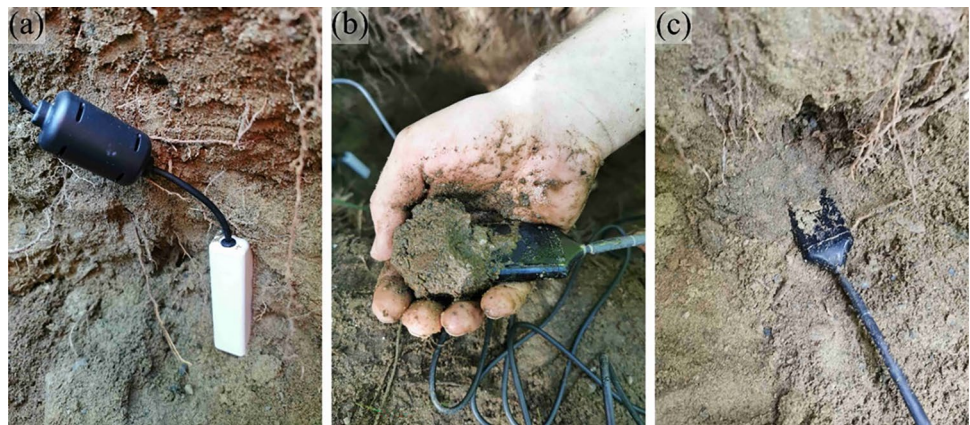
Fig. 9 Location 1: IoT-based hydrological monitoring system: **a** sensor column with soil stratigraphy, **b** aerial picture with Quaternary map, **c** monitoring point D1.2, and **d** weather station

to capture some of the nonlinearity of the infiltration process. In Location 1, the fluvial deposits were found to be much thicker, and the piezometers were placed at deeper depths to monitor potential long-term groundwater table variations and pore water pressure buildup.

In Location 1, the IoT-based hydrological monitoring setup is the full setup including two piezometers, three suction sensors, and three VWC sensors (Fig. 9a). Piezometers were placed at 1.25 m and 2.0 m depths at monitoring points D1.1 and at 1.4 m and 2.2 m depths at monitoring points D1.2 (Fig. 9b). Sand was filled as a filtering medium around the piezometers. On top of the sand fill, 10–20 cm bentonite was placed to prevent any vertical water passage. The pairs of VWC and suction sensors were installed at approximately three depths: 0.3 m, 0.5 m, and 0.9 m. VWC sensors were installed carefully to the sidewall of the excavated pit

until the needles are fully inside the original undisturbed soil (Fig. 10a). For the suction sensors, a small hole was created at the sidewall, and the soil around the sensor was moisturized to obtain good contact between the sensor and the soil. Then, the moisturized soil was packed around the entire sensor discs to ensure full contact (Fig. 10b), and it was placed back to the hole on the sidewall (Fig. 10c). After the placement of a pair of sensors, the excavated pit was backfilled to preserve the in situ bulk density of the soil using the excavated soil until the next level of sensors. The IoT Device was attached to a tree or a pole at approximately 1 m above the ground surface near the monitoring point as shown in Fig. 9c. Finally, the sensor cables were connected to the IoT Device via cable trenches and a PVC pipe along the pole.

Fig. 10 **a** Placement of VWC sensor, **b** packing moisturized soil around the discs of the suction sensor, and **c** placement of the suction sensor



As shown in Fig. 11, the IoT-based hydrological monitoring setup, in Location 2, is the reduced setup including three suction sensors, and three VWC sensors at each monitoring point: D2.1 and D2.2. The abovementioned installation procedures have been followed during the installation of the VWC and suction sensors. At point D2.2 (Fig. 11b), the presence of the bedrock has been observed at approximately 1 m depth.

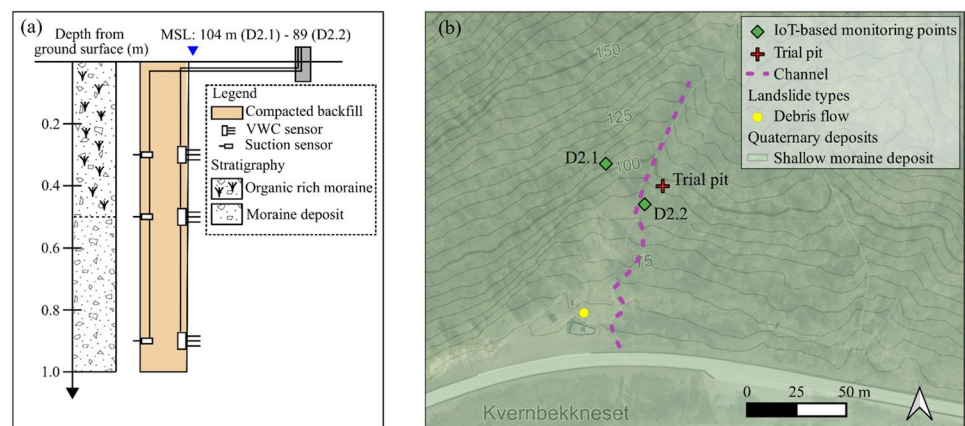
Data acquisition and interpretation of collected data

The IoT-based hydrological monitoring system started collecting data on VWC, matric suction, and pore water pressure in August 2020. Apart from one occurrence of hardware failure immediately after deployment, which was solved by replacing the faulty hardware, and a few instances of a short-term network outage, the system operated with no significant downtime. Additionally, it should be noted that the weather data could not be retrieved for February 2021 due to a loose cable connection. The missing weather data, such as precipitation, air temperature, and atmospheric pressure have been collected from nearby weather stations. In this section, all

monitored data are presented and interpreted in the following paragraphs.

Figure 12 shows the air temperature and daily precipitation data from the weather station. In Fig. 12a, the ground temperature data retrieved from the suction sensors at D1.2 (Fig. 9b) are also provided for comparison purposes. The sensors at other monitoring points provided similar ground temperature values compared to the suction sensors at D1.2. The average air temperature was approximately 6 °C over the monitoring period and varied in the range from -20 °C to +30 °C. The air temperature was significantly below 0 °C in January and February 2021 with an average of approximately -7 °C. Then, the air temperature started to rise above 0 °C from March 2021. Figure 12a shows that the ground temperature was more stable on short temporal scales compared to the variations in the air temperature. It was observed that the ground temperature generally decreased with depth when the air temperature was above 0 °C. This trend reversed in October 2020 as the air temperature started decreasing. In the cold season, from mid-October to almost April, the ground temperature increased with depth. Similar trends in ground temperature with depth were reported in the study of Bordoni et al. (2021). For the 1-year monitoring data starting from August 2020, the total

Fig. 11 Location 2: IoT-based hydrological monitoring system: **a** sensor column with soil stratigraphy (D2.2), **b** aerial picture with Quaternary map



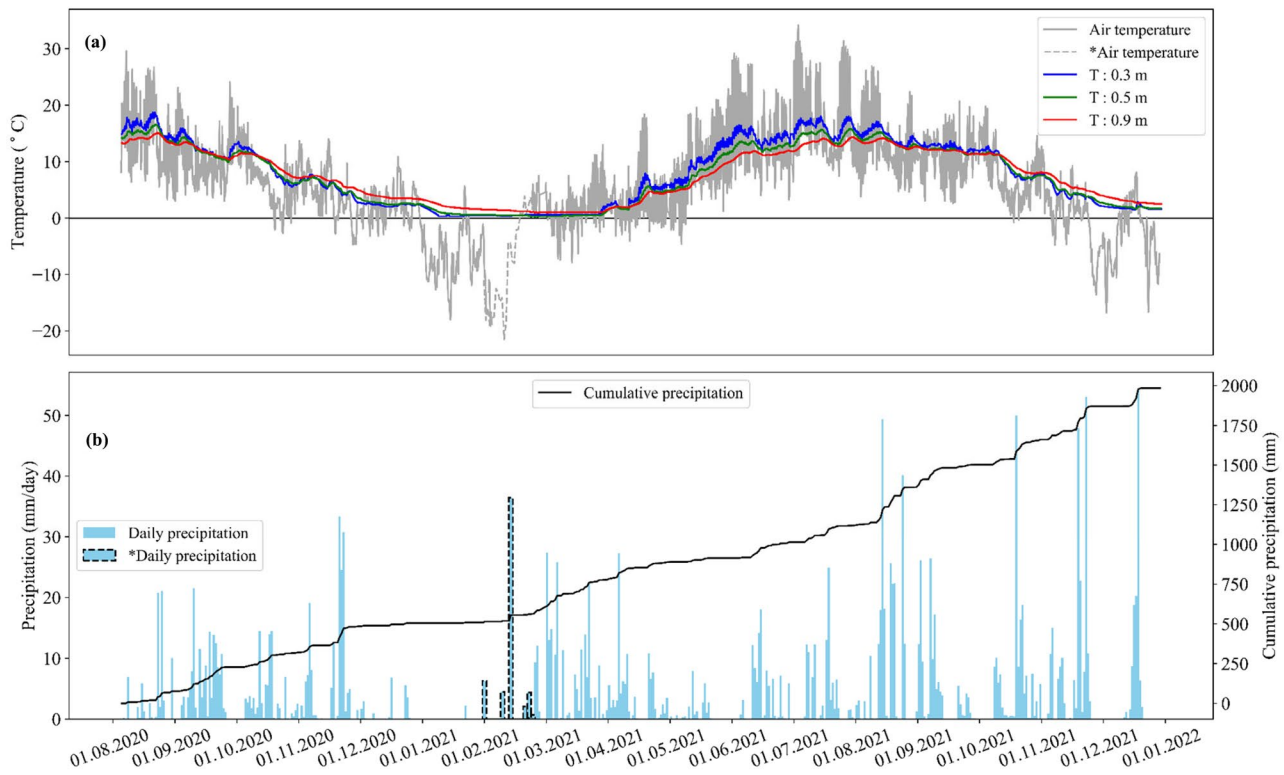


Fig. 12 Weather station data: **a** air temperature with ground temperature measurements retrieved from suction sensors at D1.2, **b** precipitation data with cumulative precipitation (*Data obtained from nearby weather stations)

cumulative rainfall is 1138 mm which is consistent with the value of 1053 mm recorded at the nearby weather station for the same monitoring period. From Fig. 12b, it can be seen that there was less rainfall from mid-November 2020 to mid-February 2021 in the winter period.

Figures 13 and 14 show the data retrieved from the VWC and suction sensors at all four monitoring points: D1.1 and D1.2 in Fig. 13 and D2.1 and D2.2 in Fig. 14. Both figures provide VWC data with the precipitation data from the weather station. The VWC sensor data were converted from sensor output in mV to the VWC by using the custom calibration equations developed for moraine and fluvial deposits (the “Laboratory tests” section). The VWC values were compared to the precipitation measurements to demonstrate the effects of rainfall on the VWC profile. It was observed that the VWC sensors responded swiftly to rainfall events. That is, VWC increased following the rainfall events and decreased in periods with less or without precipitation. In the monitored period, the VWC values ranged between 0.04 and 0.27 m^3m^{-3} at D1.1, between 0.06 and 0.35 m^3m^{-3} at D1.2, between 0.09 and 0.38 m^3m^{-3} at D2.1, and between 0.07 and 0.45 m^3m^{-3} at D2.2. Distinct periods of wetting and drying were observed at each monitoring point. High values of VWC were obtained in the periods of September to December due to intense and frequent rainfall events and

mid-February to mid-April due to a combination of rainfall events and snow melt. It can be seen that the variations in the VWC data were different at different depths. Higher variations in VWC values were observed at shallow sensors, at 0.3 m depth, compared to the sensors at deeper depths with the exception of monitoring point D2.2 (Fig. 14c). At D2.2, the VWC at 0.9 m depth showed the highest variation compared to the other sensors at shallower depths. Besides, the VWC value exceeding 0.4 m^3m^{-3} was only observed at D2.2 at the deepest VWC sensor. Both high values of VWC and high variations at 0.9 m depth at D2.2 were attributed to the existence of an impermeable boundary at 1 m depth. The infiltrated water accumulated at the impermeable boundary and resulted in high VWC values. Additionally, the lateral flow might also have contributed to the VWC at the impermeable boundary. For all monitoring points, it was observed that the VWC sensors at 0.3 m depth reacted first to the rainfall events and deeper sensors started reacting with a time delay. Similar to the VWC sensors, the variations of the matric suction at three depths were different. The suction sensors at 0.3 m depth showed, in general, the highest variation in matric suction and reacted first to the rainfall events. In addition, the VWC sensors reacted faster to the rainfall events compared to the suction sensors at the same depths. In the literature, similar observations on the VWC

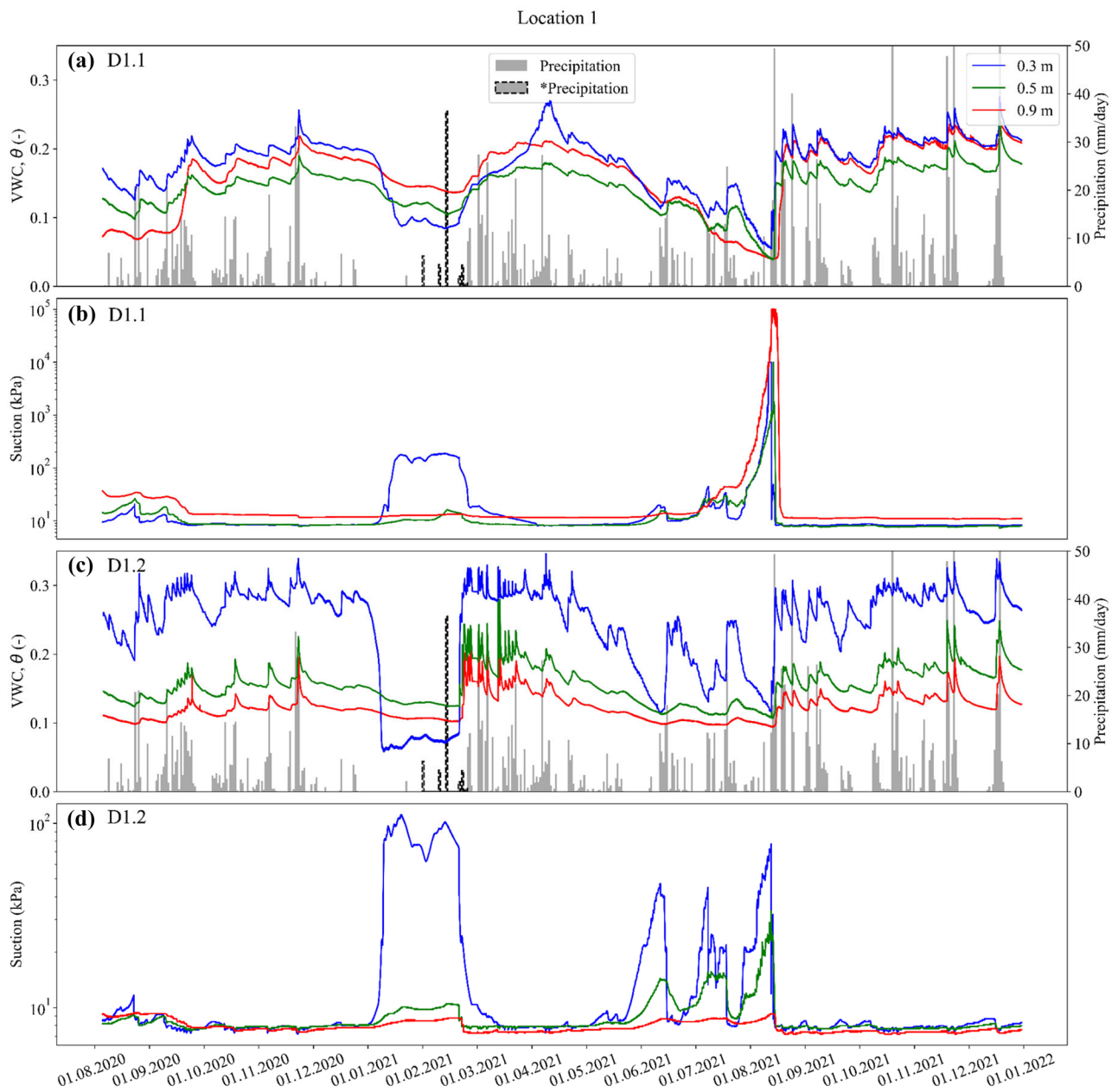


Fig. 13 VWC and suction sensor data for the monitoring points at Location 1: D1.1 **a** VWC and **b** matric suction, D1.2 **c** VWC and **d** matric suction (*Data obtained from nearby weather stations)

and suction sensor response to rainfall events, including the variations in the monitored values, changes in the response times, and variations at different depths, were reported (Comegna et al. 2016; Crawford et al. 2019; Li et al. 2005; Smith et al. 2014).

An important observation that is commonly not found in similar studies relates to the impact of the seasonally cold climate in Norway on the VWC and suction sensor readings. From both Figs. 13 and 14, it can be seen that the VWC values at 0.3 m depth dropped significantly at the beginning of January 2021 when the air temperature started

decreasing below 0 °C (Fig. 12). In the same cold period, the matric suction values at 0.3 m depth showed a sudden increase at all monitoring points. The decrease in VWC and the increase in matric suction were attributed to the freezing of the pore water at 0.3 m depth. The frozen ground at 0.3 m depth remained frozen until mid-February 2021, when the air temperature started to increase (Fig. 12). With the increase in the air temperature, the ground started to thaw. This caused an increase in the VWC and a sharp decrease in matric suction.

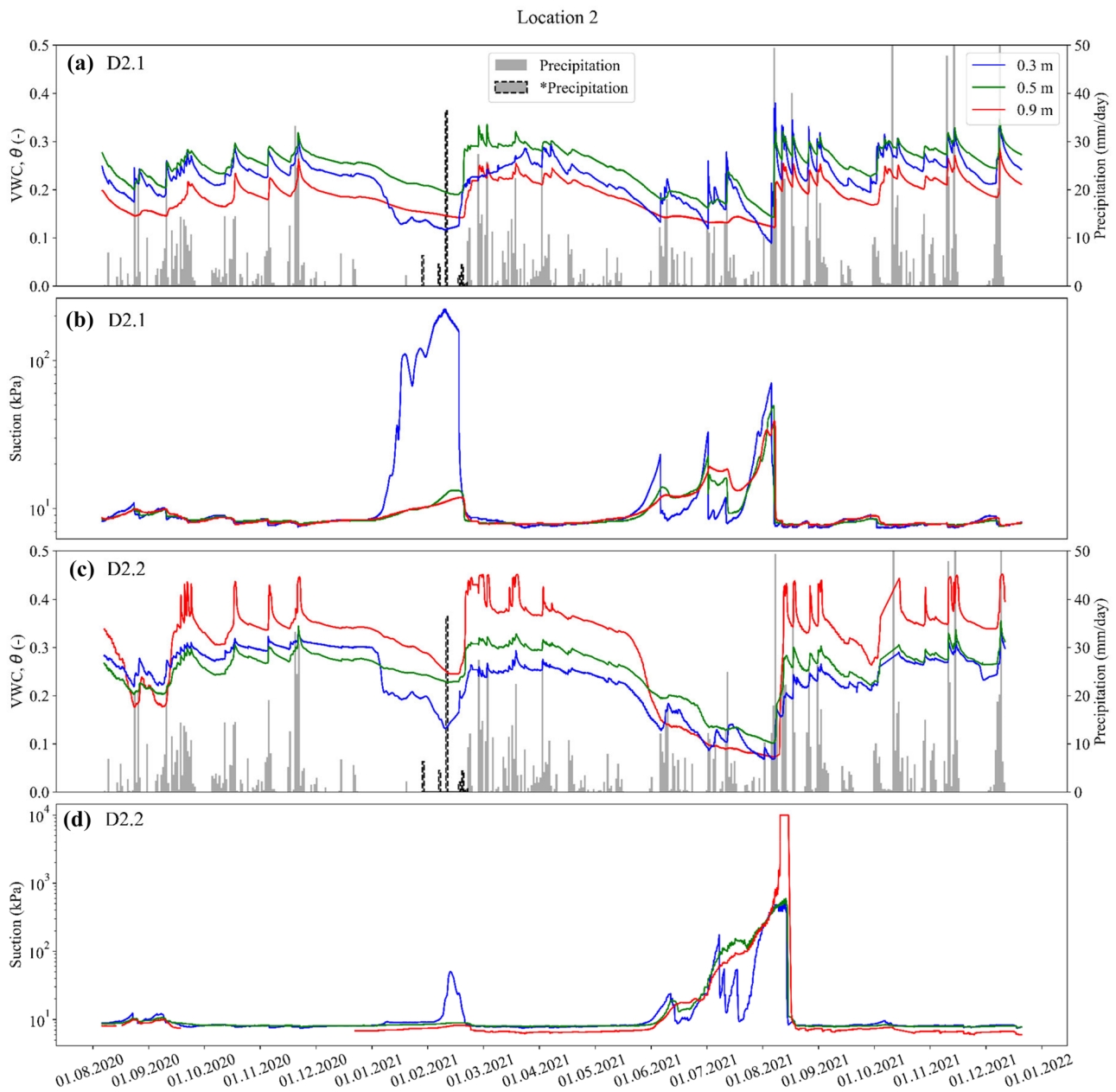


Fig. 14 VWC and suction sensor data for the monitoring points at Location 2: D2.1 **a** VWC and **b** matric suction, D2.2 **c** VWC and **d** matric suction (*Data obtained from nearby weather stations)

The matric suction values were mainly around the sensor's lower limit (9 kPa) in the periods of August to January and March to mid-May. In these periods, there were frequent rainfall events, and the VWC values were also high. Starting from mid-April 2021, a drop in VWC readings can be observed. It was attributed to the increasing air temperatures, evapotranspiration, and less frequent and less intensive rainfall events. During this dry period, the matric suction also increased considerably. The deepest suction sensors at D1.1 (Fig. 13b) and D2.2 (Fig. 14d) reached the sensor limit at

the dry state beginning of August 2021. Similarly, high matric suction values and suction values exceeding the sensor limit during the dry periods were reported in the literature (Li et al. 2005; Nunes et al. 2021; Smith et al. 2014). After mid-August 2021, the air temperature started decreasing to a milder level and larger intensity and frequency rainfall events occurred. Therefore, an increase in VWC and a decrease in matric suction values were observed.

The collected data reveals the difference in the response of VWC and suction sensors in Location 1 at D1.1 and D1.2.

The data retrieved from the sensors at D1.2 (Fig. 13c, d) show that the sensors responded even to small size precipitation events and showed higher variability at each depth. Compared to the data collected at D1.1, the VWC data at D1.2 have higher values exceeding $0.3 \text{ m}^3\text{m}^{-3}$ at the shallowest depth. These local differences in the collected data at Location 1 were attributed to the difference in the vegetation cover. While the monitoring point D1.2 has less dense vegetation cover in the form of grass (Fig. 9c), the location of D1.1 is more densely vegetated with tall trees, which prevents small precipitation amounts in easily reaching the ground. At Location 2, the main difference in the collected data, at D2.1 and D2.2, arises from the abovementioned presence of the impermeable boundary at D2.2.

The piezometer sensor readings at monitoring points D1.1 and D1.2 were converted to the pore water pressure in kPa. It was observed that the piezometer sensors have only responded to the atmospheric pressure and were not affected by the precipitation or air temperature (Fig. 12). In general, it was concluded that the converted values were not representing the pore pressure conditions at the study area and were highly under the effect of atmospheric pressure. This is likely due to very low or no groundwater levels at the positions where the piezometers were installed.

Data processing and early warning strategies

The collected data can be used in combination with data-driven or physical-based landslide prediction models to assess the landslide hazards in the study area. Assessment of landslide hazard is essential in implementing landslide risk management strategies based on monitoring and early warning solutions (Dai et al. 2002). This study features an implementation of the physical-based landslide prediction model, TRIGRS (Baum et al. 2008), to evaluate potentially unstable areas in the study area. TRIGRS is a state-of-the-art physical-based model that couples hydrological infiltration and surface runoff models with the infinite slope stability model to evaluate landslide susceptibility to storm events on local to regional levels. TRIGRS features several geotechnical and hydrological model parameters (e.g., soil strength parameters, diffusivity) that were calibrated based on the conducted laboratory and field tests and the inventory of historical landslide events in the area that were presented in earlier sections.

Landslide susceptibility assessment of the study area with TRIGRS is automated to provide predictions of potentially unstable areas for a period of 48 h based on the precipitation predictions for the study area and the sensory readings. The precipitation predictions are downloaded automatically for the study area from the weather services provided

by the Norwegian Meteorological Institute (Yr 2021). The sensory readings are used to update the initial groundwater conditions for the TRIGRS model. The initial groundwater conditions are adjusted to correspond to the average VWC values measured by the sensors in the moraine and fluvial deposit regions, respectively. The suction values are used indirectly in the updating of initial groundwater conditions by calibrating Gardner's SWCC equation in the unsaturated formulation of the TRIGRS model (Baum et al. 2008). The focus in the updating of initial groundwater conditions is on VWC sensory readings because they provide higher resolution on the part of the SWCC with low suction values. This is of high importance for wet periods of the year when most of the landslide events occur with the soil having relatively high saturation levels.

Figure 15 presents an example of the landslide susceptibility assessment of the study area with the factor of safety values for $t=0$ h, 24 h, and 48 h for the precipitation prediction shown in Fig. 15d. A factor of safety value below one indicates a landslide susceptible area, while higher values indicate increasing levels of stability. Note that the colors in the legend are only for illustration purposes to differentiate different levels of the factor of safety values and do not represent hazard or warning levels.

As seen in Fig. 15a, the slopes in the study area are stable with the majority of the factor of safety values being above 2 and the remaining between 1 and 2. Following the infiltration of the precipitation within the first 24 h, an overall decrease in the values of factor of safety can be observed with some areas having a factor of safety below one, as shown in Fig. 15b. In the following 24 h, the values of the factor of safety somewhat increase due to lower amounts of rainfall with no potentially unstable areas. These results illustrate the potential of IoT-based hydrological monitoring systems to provide relevant information that can be used in various data-driven or physical-based models to estimate landslide hazards. The system implemented in this study will be tested and developed further to contribute to the implementation of an early warning system for a regional or catchment scale and more advanced model updating strategies to integrate sensory measurements into landslide modeling.

Discussion

In the implementation of a hydrological monitoring system, it is important to have prior knowledge of the landslide events and the local geological setting of the study area. Studying landslide inventory is essential to understand the most frequent type of landslides with the corresponding initiation mechanism and triggering conditions. Additionally, landslide inventories provide a basis to interpret the frequency of sliding, expected dimensions,

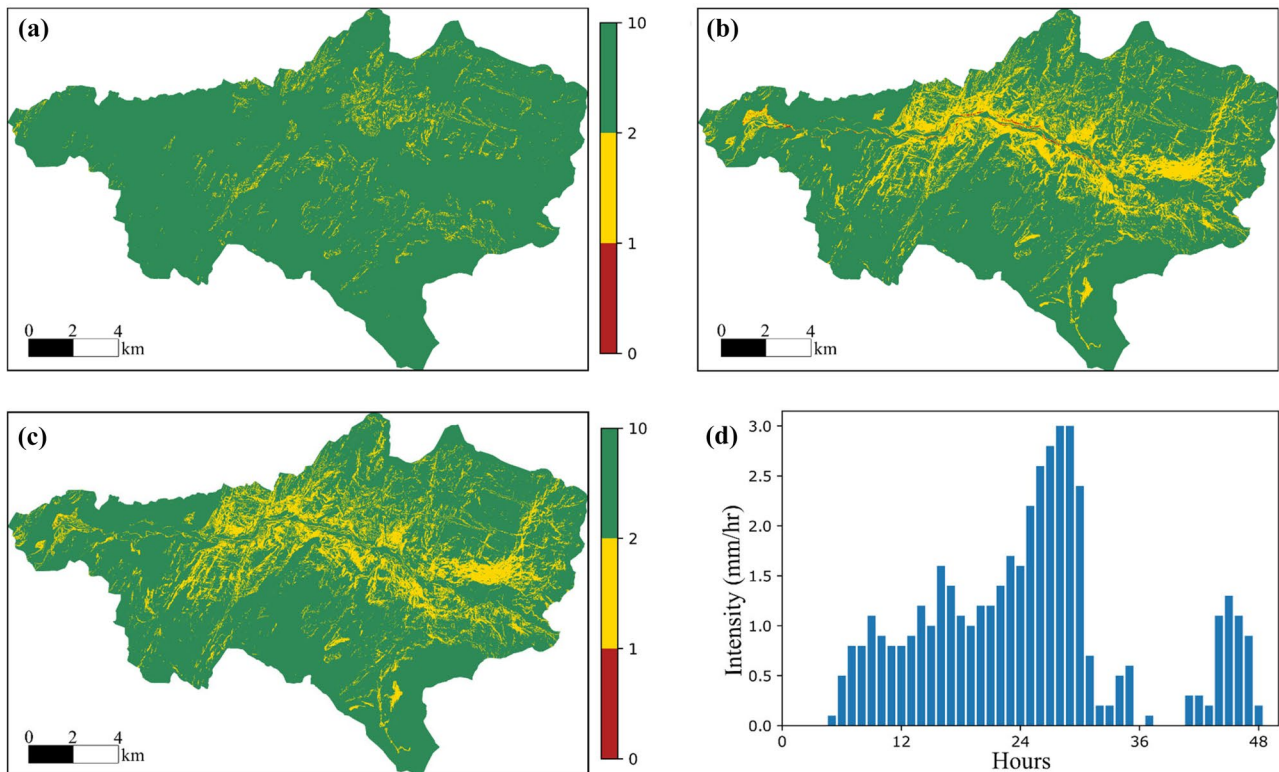


Fig. 15 Landslide susceptibility assessment of the study area with the factor of safety values for **a** $t=0$ h, **b** $t=24$ h, **c** $t=48$ h, and **d** precipitation prediction within the considered 48 h period

and the characteristics of initiation zones. Collecting and interpreting the geological information helps to identify the landslide-prone extent and to estimate the characteristics such as soil thickness and layering, geotechnical and hydrological properties, and groundwater level and flow. A comprehensive investigation of the landslide inventory and the geology is essential in determining the optimal locations to install the monitoring system and monitoring the relevant triggering conditions. While analyzing various landslide inventories, such as Norwegian database, it is important to assess the quality of the registered landslide events in the study area. Additionally, completeness of a landslide inventory is important to decide on the extent of landslide susceptible zones and locations of monitoring points. Remote sensing methods with automated advanced image processing techniques (e.g., Lu et al. 2019) have proved to be useful in developing complete landslide inventories. In a landslide inventory, errors related to the landslide location, type, and time of occurrence should be detected and corrected through quality control. Although this step is sometimes found to be tedious due to the difficulties in collecting additional information, it enhances the decision-making in designing and implementing a landslide monitoring system with improved and more reliable information.

The collected data on VWC and suction provided valuable insights into the hydrological response of the slopes to the seasonally cold climate in Norway. With the current sensory setup, the onset of ground freezing, and thawing were detected with the temperature sensors, while the effects of snow melting on hydrological conditions were measured with the VWC and suction sensors. One of the main findings through the monitoring system is the impact of ground freezing and thawing. At all monitoring points, the VWC values at the shallowest depth of 0.3 m dropped sharply due to the freezing of the soil crust layer, and the matric suction values increased simultaneously. Then, opposite changes were observed due to the thawing following the increase in the air temperature. The VWC data revealed that the intense and frequent rainfall events and combination of rainfall and snow melting resulted in high values of VWC in the ground. The suction sensors showed very low matric suction values over the large part of the year showing that the ground mainly had a high degree of saturation. However, very high matric suction values were also observed in the case of ground freezing and the summer period with no substantial rainfall events.

The VWC sensors were calibrated for the soil types at the locations of deployment as the readings are affected by the surrounding soil type. The calibration is highly important to understand the response; otherwise, inaccurate VWC data

might be obtained. The overall performance of the VWC and suction sensors in responding to the rainfall events and snow melting was fulfilling. One shortcoming of the sensory setup was regarded as suction sensors not covering the suction range below 9 kPa. This would be important to reveal the soil–water characteristics at highly saturated conditions. Additionally, piezometer readings were mainly affected by the fluctuations in atmospheric pressure, and no data representing the pore pressure conditions could be obtained. This was attributed to installing piezometer sensors in unsaturated zones where there was no groundwater during the monitored period.

The collected data on VWC and matric suction provided valuable information that can be utilized to reduce landslide risks in the study area through the deployment of an early warning system. Early warning systems are often employed as a cost-efficient landslide risk management measure in comparison to alternatives such as costly engineering solutions and restrictive areal planning measures (Calvello 2017; Dai et al. 2002). Monitoring the hydrological response of sloped terrain can be used in combination with physical-based or data-driven landslide models to estimate hazard levels in the area (e.g., Song et al. 2021). The estimated hazard levels can provide a basis for issuing timely warnings, for example, to evacuate people or close roads or railways to reduce the consequences. Integration of sensory data in landslide models is important to extrapolate the information on hydrological conditions from several monitoring locations to the study area spanning several hundreds of square kilometers. Such integration will be crucial to understand in situ conditions for an accurate prediction of landslide hazards (Abraham et al. 2020). Long-term collection of sensory data is important for developing reliable physical-based and data-driven landslide models. Physical-based landslide models have the advantage of being based on physical laws that can often provide accurate landslide predictions given the known values of various model parameters. However, these parameters are often uncertain due to the costly and time-consuming field and laboratory tests required to estimate them. Long-term data on hydrological conditions can be used to reduce uncertainties in the model parameters through the calibration of physical-based models. Similarly, long-term data can be used to improve the reliability of data-driven models by expanding the training dataset with more extreme events (e.g., rainfall with a 10-year return period).

The implemented IoT-based hydrological monitoring system has some limitations. These are reflected mainly in the limited numbers of sensors, sensory locations, and sensor types. Additional sensory locations across the study area with more sensors per location would contribute to obtaining better insight into the variations of various triggering parameters across the relatively large study area. Similarly, monitoring additional important parameters such as slope

deformations and snow amounts would be of great importance for detecting the onset of slope failure and predicting the slope stability conditions during soil thawing and snow melting events. As indicated earlier, these events present some of the most critical triggering conditions for landslides in the study area.

Typical cost components for wireless communication are device costs, infrastructure costs, subscription costs, deployment costs, and maintenance costs. The connectivity expenses of an IoT system will thus vary depending on the selected communication technology and on the possibility of employing existing communication infrastructures. In this study, a 4G-based communication solution based on low power wide area networks proved to be cost-efficient with no infrastructure costs and low costs for devices, subscriptions, deployment, and maintenance. Regarding deployment and operation of the 4G-based IoT Devices, this proved both effortless and reliable. During the system operation, some of the IoT Devices experienced minor periods of network outage, but nothing that reduced the quality of the data acquisition. If the IoT Devices were a part of an operational early warning system, such outages would however be more critical, particularly if they happen during periods of increased landslide risk. A major task for further development and implementation hence is to provide robust and resilient elements throughout the whole system. Thus, an IoT ecosystem that addresses safety issues may require a more formal collaboration with the mobile network operators, to ensure reliable operation. Although the system performance after 1 year seems promising, monitoring systems are often designed and developed for long-term monitoring over several years or decades. Similarly, the performance of the implemented system will be monitored in the years to come. Additionally, the authors expect that the continuous evolution and rapid development within IoT technology will allow for further optimizations of IoT-based hydrological monitoring systems in terms of efficiency and reliability.

Regarding the development of the IoT ecosystem, selecting a suitable communication solution will be a fundamental task that lays the foundation for several other activities throughout the lifespan of the system. As this study aimed at employing the public mobile network, its focus was exclusively on 4G-based solutions. Still, there is a need to make a decision on whether to support NB-IoT, LTE-M, or both. One would also need to ensure that the relevant mobile communication services are deployed in the field of interest and that the mobile network operators provide suitable subscriptions. If considering international deployments, one may also want to consider subscriptions with roaming agreements, thus lowering the cost and effort for entering a global market. While these questions, at first sight, may seem quite intelligible, they may however be affected by both the technological and commercial development in the

mobile network sector. As the global IoT market is expected to grow more than 20% annually over the next 5–10 years (Gartner 2019), one should be aware of the risk that network operators, and technology providers may focus on short-term benefits and strategic positioning, instead of long-term customer benefit. Therefore, doing elaborate considerations on the long-term requirements of an IoT ecosystem may be beneficial, to ensure settling for a communication solution that is as sustainable and future-proof as possible.

Summary

This study provided an overview of a case study on IoT-based hydrological monitoring of water-induced landslides in central Norway and highlighted several important findings on the implementation of IoT-based monitoring systems. The system utilized the state-of-the-art IoT technology that employs 4G public mobile networks. This provided an effortless monitoring operation with automated real-time data collection. The monitoring locations were decided through a detailed investigation of the study area in terms of geological setting and landslide inventory. The collected data on hydrological activities in terms of VWC and matric suction provided novel and valuable insights into the hydrological responses of slopes in seasonally cold climates. The effects of rainfall, snow melting, ground freezing, and ground thawing on the monitored parameters were observed. Very high values of volumetric water content were observed during the periods of snow melting or rainfall. The collected data and gained knowledge on the hydrological response of the slopes can be of high value to future efforts in reducing landslide risks through early warning system and supporting digital transformation in managing geohazards risks with IoT technologies. Besides, the current study provided an example of how the collected data could be used to obtain better hazard assessments for a regional scale early warning system.

Acknowledgements The authors acknowledge support from the R&D project KlimaDigital (2018–2022, grant number: 281059) that is funded by the Research Council of Norway and several public and private partners. The authors also acknowledge the support through project KK.01.1.1.02.0027 that is financed by the Croatian Government and the European Union through the Regional Development Fund — the Competitiveness and Cohesion Operational Programme.

Author contribution Emir Ahmet Oguz: Conceptualization; methodology; software; validation; formal analysis; investigation; resources; data curation; writing, original draft; writing, review and editing; visualization. Ivan Depina: Conceptualization; methodology; software; validation; formal analysis; investigation; resources; data curation; writing, review and editing; supervision; project administration; funding acquisition. Bård Myhre: Software, validation; writing, original draft; writing, review and editing; visualization. Graziella Devoli:

Investigation, writing, review and editing; visualization. Helge Rustad: Software, validation, investigation, writing, review and editing. Vikas Thakur: Conceptualization; resources; writing, review and editing; supervision; funding acquisition.

Funding Open access funding provided by NTNU Norwegian University of Science and Technology (incl St. Olavs Hospital - Trondheim University Hospital). The research is funded by the R&D project KlimaDigital (2018–2022, grant number: 281059).

Declarations

Conflict of interest The authors declare no competing interests.

Open Access This article is licensed under a Creative Commons Attribution 4.0 International License, which permits use, sharing, adaptation, distribution and reproduction in any medium or format, as long as you give appropriate credit to the original author(s) and the source, provide a link to the Creative Commons licence, and indicate if changes were made. The images or other third party material in this article are included in the article's Creative Commons licence, unless indicated otherwise in a credit line to the material. If material is not included in the article's Creative Commons licence and your intended use is not permitted by statutory regulation or exceeds the permitted use, you will need to obtain permission directly from the copyright holder. To view a copy of this licence, visit <http://creativecommons.org/licenses/by/4.0/>.

References

- Abraham MT, Satyam N, Pradhan B, Alamri AM (2020) Iot-based geotechnical monitoring of unstable slopes for landslide early warning in the Darjeeling Himalayas. *Sensors (switzerland)*. <https://doi.org/10.3390/s20092611>
- Anumalla S, Ramamurthy B, Gosselin DC, Burbach M (2005) Ground water monitoring using smart sensors. 2005 IEEE Int Conf Electro Inf Technol. <https://doi.org/10.1109/eit.2005.1626962>
- ASTM D3080/D3080M–11 (2021) Standard test method for direct shear test of soils under consolidated drained conditions. 9. https://doi.org/10.1520/D3080_D3080M-11
- ASTM D5030/D5030M-21 (2021) Standard test methods for density of in-place soil and rock materials by the water replacement method in a test pit. https://doi.org/10.1520/D5030_D5030M-21
- Baum BRL, Savage WZ, Godt JW (2008) TRIGRS—a Fortran program for transient rainfall infiltration and grid-based regional slope-stability analysis, version 2.0
- Bhosale A, Nimbore P, Shitole S, Govindwar O (2017) Landslide monitoring system using IoT. *IOP Conf Ser Mater Sci Eng* 263:999–1002. <https://doi.org/10.1088/1757-899X/263/4/042027>
- Bordoni M, Bittelli M, Valentino R, Vivaldi V, Meisina C (2021) Observations on soil-atmosphere interactions after long-term monitoring at two sample sites subjected to shallow landslides. *Bull Eng Geol Environ* 80:7467–7491. <https://doi.org/10.1007/s10064-021-02334-y>
- Bordoni M, Meisina C, Valentino R, Lu N, Bittelli M, Chersich S (2015) Hydrological factors affecting rainfall-induced shallow landslides: from the field monitoring to a simplified slope stability analysis. *Eng Geol* 193:19–37. <https://doi.org/10.1016/j.enggeo.2015.04.006>
- Calvello M (2017) Early warning strategies to cope with landslide risk. *Riv Ital Di Geotec* 51:63–91. <https://doi.org/10.19199/2017.2.0557-1405.063>

- Chaturvedi P, Thakur KK, Mali N, Kala VU, Kumar S, Yadav S et al (2018) A low-cost IoT framework for landslide prediction and risk communication. *Internet Things A to Z* p 593–610. <https://doi.org/10.1002/9781119456735.ch21>
- Comegna L, Damiano E, Greco R, Guida A, Olivares L, Picarelli L (2016) Field hydrological monitoring of a sloping shallow pyroclastic deposit. *Can Geotech J* 53:1125–1137. <https://doi.org/10.1139/cgj-2015-0344>
- Crawford MM, Bryson LS, Woolery EW, Wang Z (2019) Long-term landslide monitoring using soil-water relationships and electrical data to estimate suction stress. *Eng Geol* 251:146–157. <https://doi.org/10.1016/j.enggeo.2019.02.015>
- CRED (2021) Centre for Research on the Epidemiology of Disasters. <https://www.cred.be/>. Accessed 31 Dec 2021
- Dahlman E, Parkvall S, Skold J (2016) 4G, LTE-advanced pro and the road to 5G. Academic Press. <https://doi.org/10.1016/C2015-0-01834-2>
- Dai FC, Lee CF, Ngai YY (2002) Landslide risk assessment and management: an overview. *Eng Geol* 64:65–87. [https://doi.org/10.1016/S0013-7952\(01\)00093-X](https://doi.org/10.1016/S0013-7952(01)00093-X)
- Devoli G, Bell R, Cepeda J (2019) NVE report 1/2019: Susceptibility map at catchment level, to be used in landslide forecasting, Norway
- Devoli G, Dahl M-P (2014) NVE report 37/2014: Preliminary regionalization and susceptibility analysis for landslide early warning purposes in Norway. Oslo, Norway
- Fischer L, Rubensdotter L, Sletten K, Stalsberg K, Melchiorre C, Horton P, and Jaboyedoff M (2012) Debris flow modeling for susceptibility mapping at regional to national scale in Norway. In *Proceedings of the 11th International and 2nd North American Symposium on Landslides* (pp. 3–8).
- Froude MJ, Petley DN (2018) Global fatal landslide occurrence from 2004 to 2016. *Nat Hazards Earth Syst Sci* 18:2161–2181. <https://doi.org/10.5194/nhess-18-2161-2018>
- Gartner (2019) Press release: Gartner Says 5.8 Billion enterprise and automotive IoT endpoints will be in use in 2020. <https://www.gartner.com/en/newsroom/press-releases/2019-08-29-gartner-says-5-8-billion-enterprise-and-automotive-iiot>. Accessed 11 Aug 2021
- Geonor (2021) Geonor M-600 series high performance piezometer. <https://www.geonor.no/produkter/poretrykkmalere>. Accessed 31 Dec 2021
- Godt JW, Baum RL, Lu N (2009) Landsliding in partially saturated materials. *Geophys Res Lett* 36:1–5. <https://doi.org/10.1029/2008GL035996>
- Haque U, da Silva PF, Devoli G, Pilz J, Zhao B, Khaloua A et al (2019) The human cost of global warming: Deadly landslides and their triggers (1995–2014). *Sci Total Environ* 682:673–684. <https://doi.org/10.1016/j.scitotenv.2019.03.415>
- Höglund A, Lin X, Liberg O, Behravan A, Yavuz EA, Van Der Zee M et al (2017) Overview of 3GPP release 14 enhanced NB-IoT. *IEEE Netw* 31:16–22. <https://doi.org/10.1109/MNET.2017.1700082>
- Hou X (2018) Geotechnical engineering slope monitoring based on internet of things. *Int J Online Biomed Eng* 14:165–176. <https://doi.org/10.3991/ijoe.v14i06.8706>
- ISO 14688–2:2017 (2017) Geotechnical investigation and testing — identification and classification of soil — Part 2: Principles for a classification
- ITU (2012) Overview of the Internet of things (recommendation ITU-T Y.2060)
- Khaing CC, Thein TLL (2020) Prediction of rainfall based on deep learning and internet of things to prevent landslide. *2020 IEEE 9th Glob Conf Consum Electron GCCE: 190–1*. <https://doi.org/10.1109/GCCE50665.2020.9292057>
- Kim K, Jeong S, Song Y, Kim M, Park J (2021) Four-year monitoring study of shallow landslide hazards based on hydrological measurements in a weathered granite soil slope in South Korea
- Lacasse S, Nadim F, Kalsnes B (2010) Living with landslide risk. *Geotech Eng J SEAGS AGSSEA* 41
- Li AG, Yue ZQ, Tham LG, Lee CF, Law KT (2005) Field-monitored variations of soil moisture and matric suction in a saprolite slope. *Can Geotech J* 42:13–26. <https://doi.org/10.1139/t04-069>
- Lu N, Godt J (2008) Infinite slope stability under steady unsaturated seepage conditions. *Water Resources Research* 44:1–13. <https://doi.org/10.1029/2008WR006976>
- Lu P, Qin Y, Li Z, Mondini AC, Casagli N (2019) Landslide mapping from multi-sensor data through improved change detection-based Markov random field. *Remote Sens Environ* 231:111235. <https://doi.org/10.1016/j.rse.2019.111235>
- Mekki K, Bajic E, Chaxel F, Meyer F (2019) A comparative study of LPWAN technologies for large-scale IoT deployment. *ICT Express* 5:1–7. <https://doi.org/10.1016/j.ict.2017.12.005>
- METER Group (2021a) Teros 12 Manual. <https://www.metergroup.com/environment/products/teros-12/>. Accessed 31 Dec 2021
- METER Group (2021b) Teros 21 Manual. <https://www.metergroup.com/environment/products/teros-21/>. Accessed 31 Dec 2021
- Michoud C, Bazin S, Blikra LH, Derron MH, Jaboyedoff M (2013) Experiences from site-specific landslide early warning systems. *Nat Hazards Earth Syst Sci* 13:2659–2673. <https://doi.org/10.5194/nhess-13-2659-2013>
- Nadim F, Kjekstad O, Peduzzi P, Herold C, Jaedicke C (2006) Global landslide and avalanche hotspots. *Landslides* 3:159–173. <https://doi.org/10.1007/s10346-006-0036-1>
- Nordic Semiconductor (2021). nRF9160. <https://www.nordicsemi.com/Products/nRF9160>. Accessed 29 Jul 2021
- Nunes GB, de Oliveira OM, Massocco NS, dos Reis Higashi RA (2021) Study of the influence of suction profile seasonal variations in the global sliding safety factor of a granite residual soil slope. *Bull Eng Geol Environ* 80:7253–7267. <https://doi.org/10.1007/s10064-021-02367-3>
- Oguz EA, Robinson K, Depina I, Thakur V (2019) IoT-based strategies for risk management of rainfall-induced landslides: a review. *7th Int Symp Geotech Saf Risk (ISGSR 2019)* p 733–8. <https://doi.org/10.3850/978-981-11-2725-0-is13-2-cd>
- Pathania A, Kumar P, Sihag P, Chaturvedi P, Singh R, Uday K et al (2020) A low cost, sub-surface IoT framework for landslide monitoring, warning, and prediction. *2020 Int Conf Adv Comput Commun Embed Secur Syst*
- Pecoraro G, Calvello M, Piciullo L (2018) Monitoring strategies for local landslide early warning systems. *Landslides*. <https://doi.org/10.1007/s10346-018-1068-z>
- Petley D (2012) Global patterns of loss of life from landslides. *Geology* 40:927–930. <https://doi.org/10.1130/G33217.1>
- Ray PP (2018) A survey on internet of things architectures. *J King Saud Univ Comput Inf Sci* 30:291–319. <https://doi.org/10.1016/j.jksuci.2016.10.003>
- SafeLand (2012) Living with landslide risk in Europe: assessment, effects of global change, and risk management strategies. Deliverable 4.6: Report on evaluation of mass movement indicators
- Smith JB, Godt JW, Baum RL, Coe JA, Burns WJ, Lu N et al (2014) Hydrologic monitoring of a landslide-prone hillslope in the Elliott state forest, Southern Coast Range, Oregon, 2009–2012. <https://doi.org/10.3133/ofr20131283>
- Soegoto ES, Fauzi FA, Luckyardi S (2021) Internet of things for flood and landslide early warning. *J Phys Conf Ser*. <https://doi.org/10.1088/1742-6596/1764/1/012190>
- Song YS, Chae BG, Kim KS, Park JY, Oh HJ, Jeong SW (2021) A landslide monitoring system for natural terrain in Korea: development and application in hazard evaluations. *Sensors* 21:1–22. <https://doi.org/10.3390/s21093040>
- Sruthy MR, Anjana R, Archana R, Dhanya V, Hridya AH (2020) IoT based landslide detection and monitoring system. *Int J Res Eng Sci Manag*: 596–9

- The Norwegian Water Resources and Energy Directorate - NVE. skredregistrering n.d. www.skredregistrering.no. Accessed 14 Sep 2021
- Trimble Water (2021) Wireless Aquifer Level Monitoring. <https://www.trimblewater.com/wireless-aquifer-level-monitoring>. Accessed 28 Jul 2021
- Wei X, Fan W, Cao Y, Chai X, Bordoni M, Meisina C et al (2020) Integrated experiments on field monitoring and hydro-mechanical modeling for determination of a triggering threshold of rainfall-induced shallow landslides. A case study in Ren River catchment, China. *Bull Eng Geol Environ* 79:513–532. <https://doi.org/10.1007/s10064-019-01570-7>
- Worldsensing (2021) Remote wireless tunnel monitoring of ground water and pore pressure. <https://www.worldsensing.com/success-story/groundwater-monitoring-fornebu-metro-oslo-norway-2/>. Accessed 28 Jul 2021
- Yang Z, Cai H, Shao W, Huang D, Uchimura T, Lei X et al (2019) Clarifying the hydrological mechanisms and thresholds for rainfall-induced landslide: in situ monitoring of big data to unsaturated slope stability analysis. *Bull Eng Geol Environ* 78:2139–2150. <https://doi.org/10.1007/s10064-018-1295-5>
- Yr (2021) Free weather data service from Yr. <https://hjelp.yr.no/hc/en-us/articles/360001940793-Free-weather-data-service-from-Yr>. Accessed 22 Aug 2021